Long lifetime of the E_{1u} in-plane infrared-active modes of *h*-BN

Alfredo Segura
Departamento de Física Aplicada-ICMUV, Malta-Consolider Team, Universitat de València, Burjassot, Spain

Ramon Cuscó
Institut Jaume Almera (ICTJA-CSIC), Consejo Superior de Investigaciones Científicas, Lluís Solé i Sabarís s.n., 08028 Barcelona, Spain

Takashi Taniguchi
International Center for Materials Nanoarchitectonics, National Institute for Materials Science,1-1 Namiki, Tsukuba 305-0044, Japan

Kenji Watanabe
Research Center for Functional Materials, National Institute for Materials Science, 1-1 Namiki, Tsukuba 305-0044, Japan

Luis Artús
Institut Jaume Almera (ICTJA-CSIC), Consejo Superior de Investigaciones Científicas, Lluís Solé i Sabarís s.n., 08028 Barcelona, Spain

(Received 14 April 2020; revised manuscript received 29 May 2020; accepted 1 June 2020; published 15 June 2020)

We present an infrared reflectivity study of the E_{1u} *in-plane* phonons of hexagonal BN as a function of temperature in the 40–680 K range. The infrared reflectance spectra of high-quality lamellar single crystals are accurately fitted using Lowndes' factorized form of the dielectric response, where the longitudinal-optic (LO) frequency is an independent adjustable parameter. From this analysis we obtain reliable values for the phonon damping of the IR-active E_{1u} phonons which couple to light and give rise to the phonon-polariton excitations in this hyperbolic material. Anharmonic coupling potentials are estimated from the temperature dependence of the damping parameters. The E_{1u}(LO) mode exhibits a substantially longer lifetime than its transverse-optic counterpart, as it is basically unaffected by isotopic-disorder scattering owing to the low density of phonon states around the E_{1u}(LO) frequency.

DOI: 10.1103/PhysRevB.101.235203

I. INTRODUCTION

In recent years, *h*-BN has emerged as a revolutionary material in the field of optical [1,2] and nanophotonics [3,4] applications because of its unique properties [5]. The highly anisotropic structure of the lamellar *h*-BN crystal results in two well-separated reststrahlen bands associated with the *in-plane* and *out-of-plane* polar phonons. The high anisotropy of *h*-BN is reflected, not only on its giant birefringence—the largest among uniaxial semiconductors [6]—but also on its natural hyperbolic character, i.e., the change of sign of the electrical permittivity along orthogonal axes [4]. The coupling of the infrared (IR) photons with the polar modes of the *h*-BN lattice gives rise to phonon-polariton modes. These hybrid modes exhibit a highly directional propagation and support arbitrarily large wave vectors, which makes them very promising in subdiffractional IR nanophotonics and hyperlensing applications [7,8]. The polariton propagation length is a key parameter for extending the range of polaritonic applications to high transmission efficiency in waveguides, hyperlensing, or spatial filtering [9].

Given the ultraslow hyperbolic polariton propagation [10], long-lived, low-loss phonon polariton excitations are essential to achieve long propagation lengths. Since the lifetimes of the phonon polaritons are on the order of the optical phonon themselves [8], a good knowledge of the optical polar phonon lifetimes is desirable in order to accurately model hyperbolic polariton experiments. Polariton dispersion in guided surface hyperbolic polariton experiments has been simulated using a generic value of 2 cm^{-1} for the phonon damping [11], and, in some instances, the Raman linewidth of the E_{2g} mode has been taken as a first approximation for the IR-active phonon lifetime [9], on the assumption that the phonon lifetimes are roughly equivalent for E_{2g} and E_{1u} phonons. While this may be a reasonable assumption for the transverse-optic E_{1u}(TO) mode in view of its near degeneracy with the E_{2g} mode, it may not be the case for the longitudinal-optic E_{1u}(LO) mode, which lies much higher in energy in a region with a significantly lower phonon density of states. Only a precise investigation of these modes by means of IR spectroscopy can shed some light on this issue.

Early studies of the dielectric properties of *h*-BN were performed by reflection and transmission measurements on polycrystalline pyrolytic samples. These measurements yielded unrealistically high values of phonon damping and relatively similar values of the *in-plane* and *out-of-plane* dielectric constants [12], probably due to poor sample crystallinity and the angular deviation of the basal planes of the microcrystalline

domains. Recent IR reflectivity measurements on high-quality single crystals have revealed a giant anisotropy [13] and much lower phonon damping [14]. Being isotopic disorder the principal mechanism that limits the phonon lifetime in *h*-BN [15], a threefold increase in the polariton propagation length was demonstrated in nearly isotopically pure *h*-BN [9], opening prospects for the control of optical losses, which is essential for the development of phonon-polariton nanophotonic devices. In previous works, we extensively studied in detail the different mechanisms that limit the optical phonon lifetime by means of temperature-dependent Raman scattering measurements [15–19]. However, those studies addressed only the Raman-active E_{2g} mode. Here, we perform a complementary study of the temperature dependence of the IR-active E_{1u} phonons. In this paper, we present experimental spectroscopic data on the IR-phonon lifetimes that are relevant for phonon-polariton applications and give further insight into the mechanisms that limit phonon lifetimes in *h*-BN.

II. EXPERIMENT

The high-quality *h*-BN single crystals of natural isotopic composition used for these experiments were synthesized at 4.5 GPa and 1500 °C using barium boron nitride as a solvent in a modified belt-type high-pressure and high-temperature apparatus [20]. Reflectance measurements were performed by means of Fourier transform infrared spectroscopy (FTIR) using an Interspectrum TEO-400 Michelson interferometer module coupled to a noncommercial all-reflecting microscope optical bench and a 22-μm HgCdTe detector [21]. High-temperature experiments, from 300 to 680 K, were made in air by mounting the sample on a home-made resistively heated sample holder. The sample temperature was measured from the temperature dependence of a Pt100 resistance. In order to double check the sample temperature, a ruby microsphere was mounted in thermal contact with the sample, and its R1-R2 fluorescence band was measured at each temperature. An accurate measurement of the sample temperature can be obtained from both the wavelength shift of the ruby R1-R2 peaks and their intensity ratio [22]. Low-temperature measurements down to 40 K were carried out in a He-gas closed-cycle cryostat, with ZnSe windows. As in the high-temperature experiment, the sample temperature was measured both from the direct bias current of a Si diode thermometer mounted in the cryostat sample holder and from the fluorescence spectrum of a ruby microsphere. The reference spectrum to determine the sample reflectance was the reflection spectrum of a gold mirror. For high-temperature experiments in air, the gold reference was also taken in air. For low-temperature measurements inside the cryostat, a small piece of a gold mirror was stuck to the cold finger near to the sample. In this way, the reference spectrum includes the effect of the ZnSe window.

III. RESULTS AND DISCUSSION

Figure 1(a) displays the reflectance spectra at normal incidence on a *c* face with $E \perp c$, showing the reststrahlen region associated with the E_{1u} phonon and the Fabry-Perot interference pattern in the thin *h*-BN flake. Given the

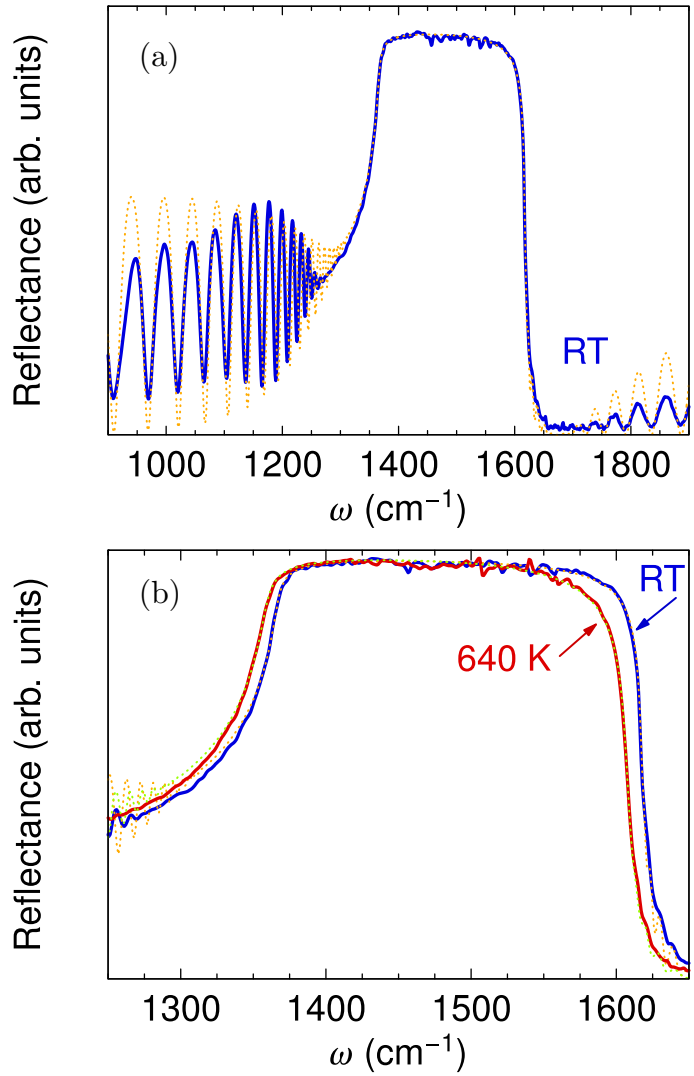

FIG. 1. (a) Infrared reflectance spectra at normal incidence ($E \perp c$) of *h*-BN at room temperature (blue solid line). The reflectance calculated using the model fit explained in the text is displayed as a yellow dotted line. (b) Expanded view of the reststrahlen band at room temperature and at 600 K illustrating the downshift of the phonon frequencies with increasing temperature.

experimental difficulties in measuring the absolute reflectance in the extremely small *h*-BN samples, the IR reflectance spectra are given in arbitrary units, since we are mainly interested in the accurate determination of the phonon parameters from the shape of the reflectance spectra. As can be seen in Fig. 1(b), the reststrahlen band, which is essentially bonded by the transverse-optic (TO) and longitudinal-optic (LO) frequencies, shows a clear downshift with increasing temperature. The analysis of the temperature dependence of the reflectance spectra can thus yield relevant information about the IR optical phonons. To model the IR spectra we employ a factorized form of the dielectric function,

$$\varepsilon(\omega) = \varepsilon_\infty \prod_{i=1}^{N} \frac{\omega_{\mathrm{LO}_i}^2 - \omega^2 - i\omega\Gamma_{\mathrm{LO}_i}}{\omega_{\mathrm{TO}_i}^2 - \omega^2 - i\omega\Gamma_{\mathrm{TO}_i}}, \tag{1}$$

where ε_∞ is the high-frequency dielectric constant, ω_{TO_i} and ω_{LO_i} are the TO and LO mode frequencies, and Γ_{TO_i} and Γ_{LO_i} are their associated dampings. Equation (1) follows from the most general form for the response function and was introduced by Lowndes [23] to study the temperature dependence of the LO frequencies and lifetimes of alkali halides. Gervais and Piriou [24] highlighted the importance of taking into account the different phonon self-energies of an LO mode compared with that of the corresponding TO mode in polar crystals with wide reflectivity bands. This is not contemplated in the classical dispersion model of harmonic oscillators, since the anharmonic coupling of phonons is neglected and the LO mode damping is not a free parameter in the classical model. When independent damping parameters Γ_{TO_i} and Γ_{LO_i} are considered in the four-parameter semiquantum (FPSQ) model, the fit to experimental data in the case of wide reflectivity bands is substantially improved. The use of the FPSQ model allowed reliable data on the TO and LO phonon lifetimes of sapphire and rutile to be extracted from infrared reflectivity experiments [24]. More recently, the same approach has been applied to the analysis of the spectroscopic ellipsometric data of sapphire [25], to attain highly accurate determinations of the dielectric function which are in excellent agreement with existing compilations in the literature.

In the reflectance spectra shown in Fig. 1, the slope at the high-frequency edge is steeper than at the low-frequency edge, suggesting that the LO phonon has a smaller damping than the TO mode. While this feature is not well reproduced by the classical dispersion model [14], the FPSQ model [Eq. (1)], in which the frequency dependence of the phonon self-energy is taken into account by considering different values of LO and TO dampings, yields a close match with the experimental reflectance data. The sample reflectance at normal incidence was calculated using Eq. (1) for $\varepsilon(\omega)$ in the model of a dielectric slab between two different media developed by Heavens [26], which also reproduces well the periodic oscillations due to the Fabry-Perot interference pattern. As can be seen in Fig. 1(b), the reflectance calculations (dotted lines) closely fit the data and accurately reproduce both edges of the reststrahlen band at all temperatures.

The values of the phonon damping parameters extracted from the fits to the reflectance data are plotted in Fig. 2. The error bars give an indication of a damping parameter range over which the FPSQ model give spectral shapes that are in reasonable agreement with the reflectance data. The damping parameter shows a steady increase as the temperature rises from 300 to 600 K, but changes little below 200 K. Experimental difficulties associated with carrying out the IR reflectivity measurements inside the cryostat limit the quality of the spectra in the low-temperature region, and thus lessen the sensitivity of the technique for detecting the small changes of the damping parameter expected for temperatures below 200 K. These limitations are more severe for the E_{1u}(TO) mode, since the low-frequency edge of the reststrahlen band is relatively broad and is more strongly affected by the interference pattern. As a consequence, the uncertainty of the low-temperature points in Fig. 2(a) is higher. Since the temperature dependence of the anharmonic damping, which determines the anharmonic model parameters, is asymptotically small at low temperatures, these low-temperature points are given a lower weight in the fitting procedure.

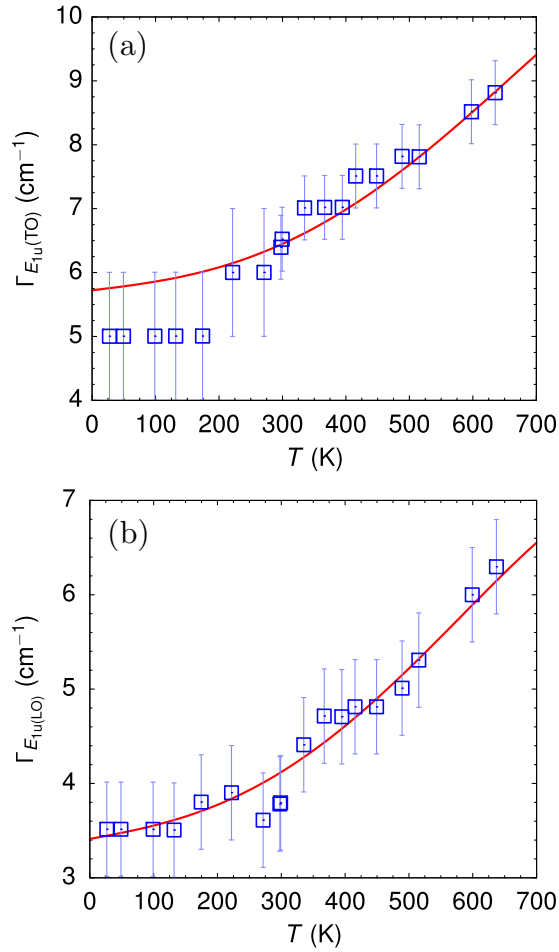

FIG. 2. (a) Temperature dependence of the damping parameter for the E_{1u}(TO) phonon. The symbols are the values extracted from the fits of the FPSQ model to the reflectance spectra. The solid line is calculated from the anharmonic decay model discussed in the text. (b) The same as (a), for the E_{1u}(LO) phonon.

The increase of the damping parameter with temperature is due to anharmonic phonon decay processes, as thoroughly discussed in Refs. [16,18,19]. By inspection of the phonon dispersion shown in Fig. 3, the dominant phonon decay paths that conserve energy and crystal momentum can be identified. The effects of phonon anharmonicity can then be modeled using a perturbation theory approach described in detail elsewhere [16,18]. Since the E_{1u}(TO) phonon is nearly degenerate with the E_{2g}^{high} Raman-active mode, essentially the same channels contribute to the anharmonic phonon decay of both modes. Thus, according to Fig. 3, we consider the three-phonon decay channel (T1)

$$E_{1u}(\mathrm{TO}) \rightarrow \begin{Bmatrix} \mathrm{LA} \\ \mathrm{LO_1} \end{Bmatrix}(K) + \begin{Bmatrix} \mathrm{ZO_1} \\ \mathrm{ZA} \end{Bmatrix}(K), \tag{2}$$

the up-conversion process (T2)

$$E_{1u}(\mathrm{TO}) \rightarrow \mathrm{LO_2}\begin{Bmatrix} (\Gamma\text{-}M) \\ (\Gamma\text{-}K) \end{Bmatrix} - \mathrm{ZA}\begin{Bmatrix} (\Gamma\text{-}M) \\ (\Gamma\text{-}K) \end{Bmatrix}, \tag{3}$$

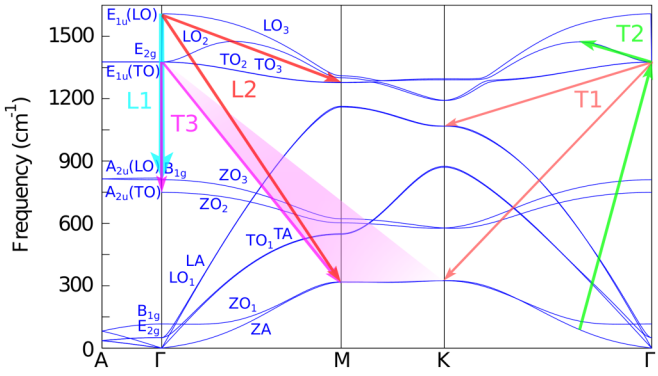

FIG. 3. Phonon dispersion of *h*-BN and dominant phonon decay channels for the E_{1u}(TO) phonon (T1, T2, T3) and for the E_{1u}(LO) phonon (L1, L2). All phonons along the *M*-*K* line can contribute to the T3 pathway (shaded area).

and the dominant four-phonon channel (T3)

$$E_{1u}(\mathrm{TO}) \rightarrow A_{2u}(\mathrm{TO}) + \begin{Bmatrix} \mathrm{ZA} \\ \mathrm{ZO_1} \end{Bmatrix}(M\text{-}K) + \begin{Bmatrix} \mathrm{ZA} \\ \mathrm{ZO_1} \end{Bmatrix}(M\text{-}K) \qquad (4)$$

that were also identified as the dominant decay pathways for the E_{2g}^{high} mode [16].

The perturbation theory calculations for the temperature dependence of the E_{1u}(TO) damping were fitted to the IR data and the result is plotted as a red solid curve in Fig. 2(a). The effective anharmonic potentials used to obtain this curve are listed in Table I. The values of the anharmonic potentials are very similar to those found for the E_{2g}^{high} phonon [18].

Since the E_{1u}(LO) phonon lies at a significantly higher frequency, the dominant decay pathways are different from those of the E_{1u}(TO) phonon. Notably, the four-phonon process (T3) that strongly contributes to the E_{1u}(TO) phonon decay is irrelevant here, inasmuch as it does not fulfill energy conservation. Instead, two dominant three-phonon decay channels, L1 and L2 (see Fig. 3), are identified for the E_{1u}(LO) phonon as

$$E_{1u}(\mathrm{LO}) \rightarrow 2B_{1g}(\Gamma), \qquad (5)$$

TABLE I. Model parameters for the anharmonic phonon decay model used to fit the experimental E_{1u}(TO) and E_{1u}(LO) data. V_3^+ and V_3^- are the effective anharmonic coupling potentials for phonon sums and differences, respectively. V_4^+ is the effective anharmonic potential for the quartic decay process. The decay paths are depicted in Fig. 3. $\tilde{V}_4$ is the effective potential for the four-phonon scattering. Γ_b is the contribution to the full width at half maximum (FWHM) from residual impurities and defects including isotopic mass defects.

		$\lvert V_3^+\rvert^2$ (cm^{-2})	$\lvert V_3^-\rvert^2$ (cm^{-2})	$\lvert V_4^+\rvert^2$ (cm^{-2})	$\tilde{V}_4$ (cm^{-1})	Γ_b (cm^{-1})
	Decay path	T1	T2	T3		
E_{1u}(TO)		4.0	0.5	6.8	−2.4	2.8
	Decay path	L1	L2			
E_{1u}(LO)		2.1	5.8		−2.5	1.1

TABLE II. Frequencies, damping parameters, and phonon lifetimes for the E_{1u}(TO), E_{1u}(LO), and E_{2g} optical modes of *h*-BN at room temperature.

	ω (cm^{-1})			Γ (cm^{-1})			τ (ps)		
E_{1u}(TO)	1366[a]	1365[b]	1367[c]	6.4[a]	4.0[b]	29[c]	0.83[a]	1.33[b]	0.18[c]
E_{1u}(LO)	1617[a]	1623[b]	1610[c]	3.8[a]	4.0[b]	29[c]	1.40[a]	1.33[b]	0.18[c]
E_{2g}		1366[d]			7.5[d]			0.71[d]	

[a]This work.
[b]Reference [14].
[c]Reference [12].
[d]Reference [17].

and

$$E_{1u}(\mathrm{LO}) \rightarrow \begin{Bmatrix} \mathrm{TO_2} \\ \mathrm{TO_3} \end{Bmatrix}(M) + \begin{Bmatrix} \mathrm{ZO_1} \\ \mathrm{ZA} \end{Bmatrix}(M), \qquad (6)$$

respectively.

Fitting the anharmonic decay model with the pathways L1 and L2 to the IR reflectivity data yields the red solid curve shown in Fig. 2(b) and the effective anharmonic potentials listed in Table I. Since the E_{1u}(LO) phonon decay is governed by third-order anharmonicity, the temperature dependence of the damping parameter exhibits in this case a linear behavior for temperatures higher than ∼400 K.

The strength of third-order anharmonicity is comparable for both LO and TO modes, which display a similar temperature dependence of the damping parameter. However, the background damping parameter Γ_b, which in the present analysis accounts for both impurity/defects and isotopic-disorder scattering, is significantly lower for the LO mode (see Table I). To explain this unexpected feature, one has to bear in mind that, contrary to the E_{1u}(TO) mode, the E_{1u}(LO) phonon frequency lies in a spectral range with a very low density of phonon states [18]. This results in negligible isotopic-disorder corrections, since, to lowest order in perturbation theory, the isotopic-disorder scattering rate is proportional to the phonon density of states [27]. Therefore, in the case of E_{1u}(LO), the background damping constant $\Gamma_b = 1.1\ \mathrm{cm}^{-1}$ primarily reflects the scattering by background impurities and defects only. It is interesting to note that a similar value of $\Gamma_b = 1.3\ \mathrm{cm}^{-1}$ was determined for the E_{2g}^{high} phonon in isotopically purified *h*-BN samples [18].

Detailed Raman measurements of the E_{2g}^{high} mode revealed strong isotopic-disorder effects arising from multiple scattering [15], leading to isotopic-disorder broadenings in the order of $4\ \mathrm{cm}^{-1}$ for the natural composition sample. Given that the E_{1u}(TO) mode is nearly degenerate with the E_{2g}^{high} mode, one would expect similar corrections due to isotopic disorder for the E_{1u}(TO) linewidth. The spectral parameters of the E_{2g}^{high} and E_{1u} optical modes obtained in the present IR study and those reported in previous works are compared in Table II. The phonon frequencies show a good agreement, except for the underestimated E_{1u}(LO) frequency reported by Geick *et al.* [12], probably due to the poor quality of the early pyrolytic *h*-BN samples. An unrealistically high value of damping was also reported in those samples, which is incompatible with the large phonon-polariton propagation lengths recently measured

in h-BN [9,10]. The damping parameter reported in Ref. [14] was somewhat lower than the E_{1u}(TO) damping we find here because the classical dispersion model was employed to fit the IR reflectance, and the steeper reflectance edge at the LO frequency tended to reduce the fitted overall damping.

As reported in Table I, the background damping parameter for the E_{1u}(TO) mode extracted from the IR spectra is only $\Gamma_b = 2.8\ \mathrm{cm}^{-1}$. Considering the background damping parameter $\Gamma_b \sim 1.1\ \mathrm{cm}^{-1}$ found for the E_{1u}(LO) phonon as an estimate of the impurity/defect broadening, the isotopic-disorder contribution to the broadening of the E_{1u}(TO) phonon would be only $\Gamma_{\mathrm{iso}} \sim 1.7\ \mathrm{cm}^{-1}$. As a matter of fact, the isotopic-disorder broadening suggested by the present IR measurements agrees fairly well with the perturbation theory estimations around 2 cm^{-1} obtained for the E_{2g} mode [17]. However, the perturbation theory approach has been shown to be insufficient to describe the isotopic-disorder effects on the Raman-active mode over the whole isotopic-composition range and to underestimate the isotopic-disorder corrections [15]. While it is clear that, on account of their respective phonon density of states, isotopic disorder affects the E_{1u}(LO) and E_{2g} modes very differently, the reason for the dissimilarity in the isotopic-disorder broadening between the E_{1u}(TO) and E_{2g} modes is not apparent, and further investigations are required to clarify this issue.

E_{1u} phonon damping values much smaller than those of E_{2g} have been reported in graphite, but they were attributed to the stronger contribution of the electron-phonon mechanism in limiting the E_{2g} phonon lifetime [28]. Because of the wide band gap of h-BN, the electron-phonon mechanism is negligible in h-BN, and cannot explain the higher dampings reported for the E_{2g}^{high} mode in natural h-BN compared to the value obtained for the E_{1u}(TO) mode in the present IR measurements.

In any case, as can be see in Table II, the present IR measurements show that the lifetime of the E_{1u}(TO) mode is higher than that of the E_{2g} mode. However, isotopic disorder appears to affect more strongly the E_{2g}^{high} mode than the E_{1u}(TO) mode, which suggests that the increase of phonon lifetime of the latter that is achievable by isotopic purification may be less than anticipated from the dramatic increase of E_{2g}^{high} lifetime in isotopically pure h-BN [17].

The temperature dependence of the E_{1u} phonon frequencies is plotted in Fig. 4. Both LO and TO frequencies exhibit a similar decrease with temperature as a result of the dominant role of the four-phonon scattering contribution that reverses the increasing trend due to thermal expansion. The effective anharmonic potentials $\tilde{V}_4$ used to calculate the four-phonon scattering contribution are listed in Table I, and they are consistent with the values previously found for the E_{2g}^{high} mode [17]. The increasing frequency trend induced by the thermal expansion is smaller for the LO mode because the large increase of the c parameter with temperature reduces the density of polarizable units and tends to reduce the LO-TO splitting. As a result, the overall decrease with temperature of the LO frequency is slightly higher. As can be seen in Fig. 4(b), the contribution of anharmonic decay to the frequency shift of the E_{1u}(LO) phonon is entirely negligible. On the whole, the frequencies of the IR-active modes of h-BN display a temperature dependence very similar to that previously reported for the E_{2g}^{high} Raman-active mode.

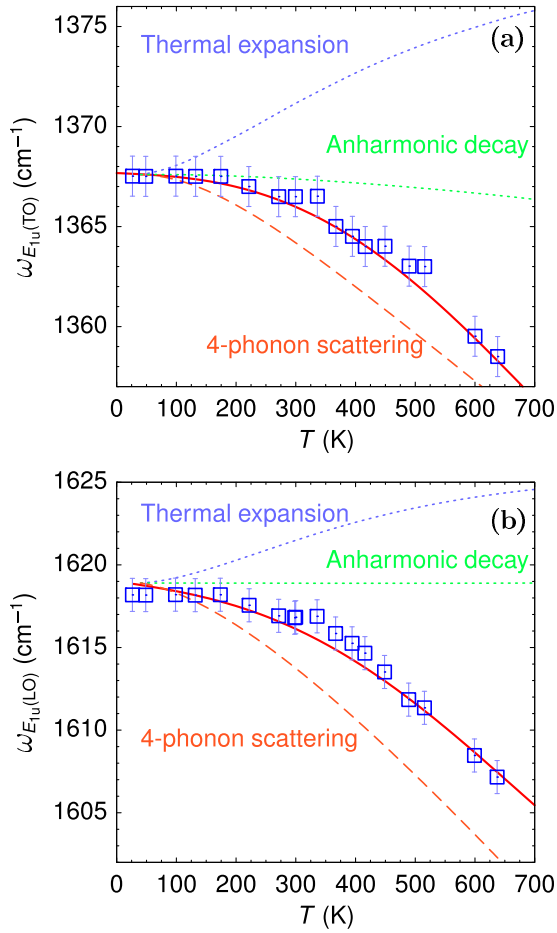

FIG. 4. (a) Temperature dependence of the E_{1u}(TO) phonon frequency. The symbols are the values extracted from the fits of the FPSQ model to the reflectance spectra. The solid red line is calculated from the anharmonic decay model discussed in the text. The separate contributions from thermal expansion, anharmonic decay, and phonon-phonon scattering are indicated by dotted and dashed lines. (b) The same as (a), for the E_{1u}(LO) phonon.

IV. CONCLUSIONS

We have presented an experimental IR reflectivity study of the phonon lifetime of the E_{1u} IR-active modes of h-BN. A FPSQ model based on Lowndes' factorized form of the dielectric response that considers independent damping parameters for TO and LO phonons, allowing for different phonon broadening mechanisms for each phonon branch, provides a better description of the wide reststrahlen band of the IR reflectance spectra than the classical dispersion model of harmonic oscillators. The FPSQ model accurately fits the low- and high-frequency edges of the restsrahlen band and allows us to extract reliable values of the TO and LO damping parameters from the IR reflectance spectra.

The reststrahlen band of the IR reflectance spectra clearly shifts to lower frequencies with increasing temperature and displays a steeper slope at the LO frequency. The analysis

of the temperature dependence of the IR reflectance spectra yields information about the anharmonic phonon decay and isotopic-disorder scattering for the IR-active E_{1u} modes, thus complementing our previous Raman scattering study of the E_{2g} modes.

The E_{1u}(TO) phonon decays through the same anharmonic channels as the E_{2g}^{high} mode. Different decay channels are identified for the E_{1u}(LO) phonon, which is found to decay basically through third-order anharmonicity. The E_{1u}(LO) phonon exhibits a significantly higher lifetime [1.4 ps at room temperature (RT)] than its TO counterpart (0.8 ps at RT) because it is essentially unaffected by isotopic disorder. In comparison with the Raman-active E_{2g}^{high} mode, the E_{1u}(TO) phonon exhibits a longer lifetime and it appears to be less sensitive to isotopic disorder. The FPSQ model fit to the IR reflectance spectra provides experimental determinations of the dampings of the E_{1u}(TO) and E_{1u}(LO) phonons. Since the polar IR-active modes are those which couple to light, the determination of these parameters is of interest for modeling phonon-polariton devices on a more realistic basis than the approaches used so far that involve using either generic guesses or extrapolations of the well-known Raman-active modes.

ACKNOWLEDGMENTS

This work has been supported by the Spanish MINECO/FEDER under Contracts No. MAT2015-71035-R and No. MAT2016-75586-C4-1-P. K.W. and T.T. acknowledge support from the Elemental Strategy Initiative conducted by the MEXT, Japan, Grant No. JPMXP0112101001, JPS, KAKENHI Grant No. JP20H00354, and the CREST (JPMJCR15F3), JST.

[1] K. Watanabe, T. Taniguchi, and H. Kanda, Nat. Mater. **3**, 404 (2004).
[2] G. Cassabois, P. Valvin, and B. Gil, Nat. Photon. **10**, 262 (2016).
[3] S. Dai, Z. Fei, Q. Ma, A. S. Rodin, M. Wagner, A. S. McLeod, M. K. Liu, W. Gannett, W. Regan, K. Watanabe *et al.*, Science **343**, 1125 (2014).
[4] J. D. Caldwell, A. V. Kretinin, Y. Chen, V. Giannini, M. M. Fogler, Y. Francescato, C. T. Ellis, J. G. Tischler, C. R. Woods, A. J. Giles *et al.*, Nat. Commun. **5**, 5221 (2014).
[5] J. D. Caldwell, I. Aharonovich, G. Cassabois, J. H. Edgar, B. Gil, and D. N. Basov, Nat. Rev. Mater. **4**, 552 (2019).
[6] A. Segura, L. Artús, R. Cuscó, R. Goldhahn, and M. Feneberg, Phys. Rev. Mater. **1**, 024604 (2017).
[7] P. Li, M. Lewin, A. V. Kretinin, J. D. Caldwell, K. S. Novoselov, T. Taniguchi, K. Watanabe, F. Gaussmann, and T. Taubner, Nat. Commun. **6**, 7507 (2015).
[8] T. Low, A. Chaves, J. D. Caldwell, A. Kumar, N. X. Fang, P. Avouris, T. F. Heinz, F. Guinea, L. Martin-Moreno, and F. Koppens, Nat. Mater. **16**, 182 (2016).
[9] A. J. Giles, S. Dai, I. Vurgaftman, T. Hoffman, S. Liu, L. Lindsay, C. T. Ellis, N. Assefa, I. Chatzakis, T. L. Reinecke *et al.*, Nat. Mater. **17**, 134 (2017).
[10] E. Yoxall, M. Schnell, A. Y. Nikitin, O. Txoperena, A. Woessner, M. B. Lundeberg, F. Casanova, L. E. Hueso, F. H. L. Koppens, and R. Hillenbrand, Nat. Photon. **9**, 674 (2015).
[11] P. Li, I. Dolado, F. J. Alfaro-Mozaz, A. Y. Nikitin, F. Casanova, L. E. Hueso, S. Vélez, and R. Hillenbrand, Nano Lett. **17**, 228 (2016).
[12] R. Geick, C. H. Perry, and G. Rupprecht, Phys. Rev. **146**, 543 (1966).
[13] A. Segura, L. Artús, R. Cuscó, T. Taniguchi, G. Cassabois, and B. Gil, Phys. Rev. Materials **2**, 024001 (2018).
[14] A. Segura, R. Cuscó, T. Taniguchi, K. Watanabe, G. Cassabois, B. Gil, and L. Artús, J. Phys. Chem. C **123**, 17491 (2019).
[15] R. Cuscó, J. H. Edgar, S. Liu, J. Li, and L. Artús, Phys. Rev. Lett. **124**, 167402 (2020).
[16] R. Cuscó, B. Gil, G. Cassabois, and L. Artús, Phys. Rev. B **94**, 155435 (2016).
[17] R. Cuscó, L. Artús, J. H. Edgar, S. Liu, G. Cassabois, and B. Gil, Phys. Rev. B **97**, 155435 (2018).
[18] R. Cuscó, J. H. Edgar, S. Liu, G. Cassabois, B. Gil, and L. Artús, Phys. Rev. B **99**, 085428 (2019).
[19] R. Cuscó, J. Edgar, S. Liu, G. Cassabois, B. Gil, and L. Artús, J. Phys. D: Appl. Phys. **52**, 303001 (2019).
[20] T. Taniguchi and K. Watanabe, J. Cryst. Growth **303**, 525 (2007).
[21] V. Panchal, A. Segura, and J. Pellicer-Porres, High Press. Res. **31**, 445 (2011).
[22] D. D. Ragan, R. Gustavsen, and D. Schiferl, J. Appl. Phys. **72**, 5539 (1992).
[23] R. P. Lowndes, Phys. Rev. B **1**, 2754 (1970).
[24] F. Gervais and B. Piriou, J. Phys. C **7**, 2374 (1974).
[25] M. Schubert, T. E. Tiwald, and C. M. Herzinger, Phys. Rev. B **61**, 8187 (2000).
[26] O. S. Heavens, *Optical Properties of Thin Solid Films* (Dover, New York, 1991).
[27] S.-I. Tamura, Phys. Rev. B **30**, 849 (1984).
[28] N. Bonini, M. Lazzeri, N. Marzari, and F. Mauri, Phys. Rev. Lett. **99**, 176802 (2007).